Magnetic field generation and diffusion by a laser-produced blast wave propagating in non-homogenous plasma

2015 New J. Phys. 17 043052

(http://iopscience.iop.org/1367-2630/17/4/043052)

IOP Publishing New J. Phys. 17 (2015) 043052 doi:10.1088/1367-2630/17/4/043052

New Journal of Physics
The open access journal at the forefront of physics

Deutsche Physikalische Gesellschaft DPG
IOP Institute of Physics

Published in partnership with: Deutsche Physikalische Gesellschaft and the Institute of Physics

OPEN ACCESS

RECEIVED
24 November 2014

REVISED
23 February 2015

ACCEPTED FOR PUBLICATION
24 March 2015

PUBLISHED
27 April 2015

PAPER

Magnetic field generation and diffusion by a laser-produced blast wave propagating in non-homogenous plasma

A Marocchino, S Atzeni and A Schiavi

Dipartimento SBAI, Università di Roma 'La Sapienza', Italy

E-mail: alberto.marocchino@uniroma1.it

Keywords: plasma physics, magnetic field self-induction, laboratory astrophysics

Abstract

In this paper we discuss the magnetic field self generation, via the so-called Biermann battery effect, and its diffusion for a blast wave (BW) expanding in a perturbed background medium. A series of simulations verify the bi-linear behavior of the Biermann battery source term both in amplitude and in wavenumber. Such a behavior is valid in the limit of no diffusivity. When diffusivity is also considered, we observe an inverse proportionality with the wavenumber: for large wavenumber perturbation magnetic diffusivity plays a key role. Writing the induction equation in a dimensionless form we discuss how, in terms of magnetic properties, the BW can be subdivided into three main regions: the remnant where the frozen-in-flow approximation holds, the thin shell where the magnetic field is in fact generated but at the same time begins to diffuse, and the shock front where the magnetic field diffuses away. A possible experimental scenario that could induce magnetic fields of about 100 gauss is finally investigated. Simulations have been performed with the code DUED.

1. Introduction

The development in high-power laser technology and in high-resolution plasma diagnostics has prompted a significant increase in the number of laser-plasma interaction experiments devoted to the investigation of astrophysical phenomena in the laboratory [1–13]. By rewriting the dynamical equations in terms of dimensionless quantities and parameters [14–16], it is possible to scale down astrophysical phenomena to the temporal and spatial scales typical of a plasma experiment in the laboratory. A laser-generated blast wave (BW) in a background gas could be used for instance to investigate the evolution of a Supernova remnant (SNR) propagating through interstellar medium [17–19].

In recent years several experiments have been devoted to uncover the mechanisms that might seed magnetic field generation in SNRs. It has been observed that the Biermann battery [1] is a possible and suitable mechanism to induce magnetic fields. The induced magnetic fields are rather weak, but it also appears plausible that, eventually, in combination with dynamo effects, fields get amplified and become rather important in the overall dynamics [1]. SNRs are reproduced in a laboratory environment as BW, a large amount of energy is instantaneously deposited in a very small region (high energy density). This procedure, relatively simple to setup, has become rather standard over the years.

In this work we present numerical investigations of the mechanisms that lead to magnetic field generation and evolution in a laser-generated cylindrical blast wave. SNRs are 3D spherical phenomena, however in this paper we consider a simplified 2D cylindrical case. Indeed a 2D scenario allows to describe the main underlying physics without loss of generality and it is simpler to reproduce experimentally. Density perturbations of the background gas seed the growth of magnetic field structures via the so called *Biermann battery effect* [20, 22–24] when the BW passes through a region of non-homogeneous plasma. (Hydrodynamic instabilities, like the Rayleigh–Taylor instability in nonlinear regimes, are also a magnetic field seeding mechanism; this process can play some role in inertial confinement fusion [21].) The generated B field is advected away with the fluid elements in regions of the plasma where the resistivity is small. There the magnetic field lines are *frozen in flow*, as

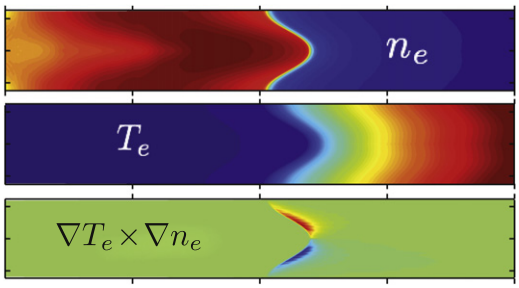

Figure 1. Snapshot of the linear phase of pure hydrodynamic RMI (data from [28]). Color maps of electron density n_e and temperature T_e are shown. The bottom panel presents the (offline computed) baroclinic source term responsible for magnetic field generation.

sometimes this phenomenon is referred to. Where instead the plasma resistivity is high, magnetic field diffusion occurs and the intensity of B is reduced via current dissipation in the plasma.

The properties of the background gas, such as chemical composition and initial density, greatly affect the generation and evolution of magnetic field structures. Also the various energy transport mechanisms present in the plasma, in particular radiative transport and non-local electron transport (NLET), play an important role in the generation of B fields induced by the BW. It is important to understand these phenomena in the laboratory, taking into account that, for instance, NLET does not scale up to astrophysical problems.

The paper is organized as follows: in the first section we describe the governing equations and their implementation in the numerical code used for the simulations. In the second section we discuss the magnetic field induction mechanism. In the third section we discuss the relative importance and contribution of the terms determining the generation and diffusion of magnetic field; in the fourth section the competition between magnetic field generation and diffusion is clarified via a systematic scan. We then present the propagation of a BW through a region of localized density perturbations, in a context similar to what could be obtained in a laser-plasma experiment. Conclusions are drawn in the last section.

2. The induction equation and the plasma model

The simulations presented in this paper are performed using DUED [25, 26] in its cylindrical version. DUED is a two-temperature Lagrangian fluid code for inertial fusion studies, it includes real matter equation of state, multigroup radiation and alpha-particle diffusion, fuel burn, three-dimensional laser ray-tracing, and inverse bremsstrahlung absorption. For electron thermal conduction DUED includes both the standard flux-limiter (sharp cutoff) technique as well as the non-local electron transport model by Schurtz–Nicolaï–Busquet [31] implemented in DUED as described in [29, 30]. The original radiative hydrodynamic version used for ICF studies has been upgraded to include the dynamical evolution of magnetic fields in a magneto-hydrodynamical approximation. The induction equation used in our analysis is based on the Ohm's law

$$\mathbf{E} = -\frac{\mathbf{u}\times\mathbf{B}}{c} + \eta\,\mathbf{J} - \frac{\nabla p_e}{e\,n_e}, \tag{1}$$

where $\mathbf{E}$ is the electric field, $\mathbf{B}$ the magnetic field, $\mathbf{J}$ the current density, p_e the electron pressure, n_e the electron number density, $\mathbf{u}$ the fluid velocity, η the plasma resistivity. Gaussian-CGS units are used throughout.

Inserting Ohm's law into Faraday's law, the magnetic induction equation is obtained

$$\frac{D}{Dt}\frac{\mathbf{B}}{\rho} = \left(\frac{\mathbf{B}}{\rho}\cdot\nabla\right)\mathbf{u} + \frac{c\,k_B}{\rho\,n_e\,e}\left(\nabla T_e\times\nabla n_e\right) - \frac{c^2}{4\pi\rho}\left(\eta\nabla^2\mathbf{B} + \nabla\eta\times\nabla\times\mathbf{B}\right), \tag{2}$$

which is written as a total derivative of $\mathbf{B}/\rho$ in the Lagrangean frame. Here ρ is the plasma mass density, and the electron pressure $p_e = n_e\,k_B T_e$ has been written as a function of electron temperature and Boltzmann constant.

The term containing $\nabla T_e \times \nabla n_e$ in equation (2) is known as the *baroclinic source term* or the *Biermann battery* term [1, 27], and it represents a magnetic field generating mechanism. The terms containing η (generally written in a compact form $\nabla\times(\eta\nabla\times\mathbf{B})$) are instead responsible for magnetic field diffusion and dissipation. The simplest case we might consider is in the absence of any source and diffusion terms, so that the quantity $\mathbf{B}/\rho$ is rigidly advected with the flow. The baroclinic term differs from zero in those regions where the electron density and temperature gradients are not parallel. An explicative example is presented in figure 1 showing a late stage of a Richtmyer–Meshkov instability [28]. In this case the cross product $\nabla T_e \times \nabla n_e$ is computed offline and plotted. The two narrow layers in which the baroclinc term generates B fields (with opposite sign) are clearly

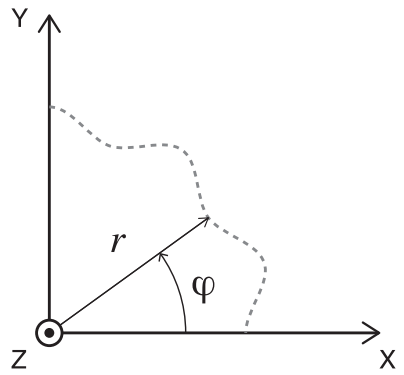

Figure 2. Axes name schematic.

visible. Magnetic field diffusivity becomes dominant in those regions where plasma temperature and characteristic gradient scale lengths are large, also when compared with fluid velocity. Magnetic field diffusion dominates over other terms in those regions where high internal energy (high temperature) has not yet converted into kinetic energy. The magnetic field is coupled to the plasma hydrodynamics in the momentum and energy equations:

$$\rho\frac{D\mathbf{u}}{Dt} = -\nabla\left(p_{\rm e} + p_{\rm i} + \frac{B^2}{8\pi}\right) + \frac{(\mathbf{B}\cdot\nabla)\mathbf{B}}{4\pi}, \tag{3}$$

$$\frac{D\varepsilon_{\rm e}}{Dt} = -p_{\rm e}\frac{D(1/\rho)}{Dt} + \frac{1}{\rho}\left(\eta J^2 - \nabla\cdot\mathbf{Q}_e - \frac{\nabla p_{\rm e}}{n_{\rm e}\, e}\cdot\mathbf{J}\right), \tag{4}$$

where $\mathbf{u}$ is the fluid velocity, $p_{\rm e}$ the electron pressure, $p_{\rm i}$ the ion pressure, $\varepsilon_{\rm e}$ the electron specific energy, $\mathbf{Q}_{\rm e}$ the heat flux and $\mathbf{J} = c/4\pi\,\nabla\times\mathbf{B}$ is the current density. The simulations were run in 2D (x, y) slab geometry, with the hydrodynamic quantities independent of the z co-ordinate. As such, the induced magnetic field has the B_z component only. Physical viscosity has been neglected since it plays practically no role for temperatures, density and time ranges considered.

The electron thermal conduction was modeled using both the standard flux-limiter technique and a NLET model [29–31]. Radiation transport is dealt with by a flux-limited multi-group diffusion scheme. Tabulated opacities are provided by an upgraded version of the SNOP code [33], which computes steady-state-non-local-thermal-equilibrium opacities using an average-atom model. Material properties are described by a tabulated equation of state [34] accounting for several non-ideal effects, including partial ionization (of particular relevance for the present study).

3. Regular density perturbation as seeding mechanism for the Biermann battery effect

To illustrate the chain process that seeds and induces the magnetic field we begin with a simplified scenario in which a BW encounters a regular density perturbation of the background medium [12, 19]. We assume that the BW is generated by the instantaneous energy deposition of an ultrashort laser pulse [32] (density and velocity evolution are plotted in figure 3 for a selection of times) propagating through a rarefied gas along the z axis, with the axis-name convention depicted in figure 2. In this section we discuss the magnetic field generation induced by the BW, neglecting B-field diffusion.

In order to shed light on the basic mechanism that leads to magnetic field generation during a BW expansion, we choose a simplified scenario, which allows us to verify a few scaling laws connected to the Biermann battery effect. Our first case study involves a BW launched in Hydrogen gas (H). The BW is initialized with a gaussian temperature profile that corresponds to the instantaneous deposition of 2 J of laser energy in a cylindrical volume 3 mm long and 60 μm wide (standard deviation). The background gas had a uniform density of 5×10^{18} cm^{-3}. A sinusoidal density perturbation of the form $\rho_0(1 + A\cos k\varphi)$ (as illustrated in [28]) is imposed in the region 800 μm $< r <$ 950 μm, where ρ_0 is the unperturbed mass density, A the modulation amplitude, k the wavenumber and φ the azimuthal angle (refer to figure 2). The simulation domain was set to the first quadrant $(0 \leqslant \varphi \leqslant \pi/2)$ with periodic boundary condition in the φ-direction. The initial grid was divided into 200 equally spaced zones in the radial direction and 64 in the azimuthal direction.

For this simple case, it is possible to perform a linear analysis of the baroclinic term in the induction equation, which leads to

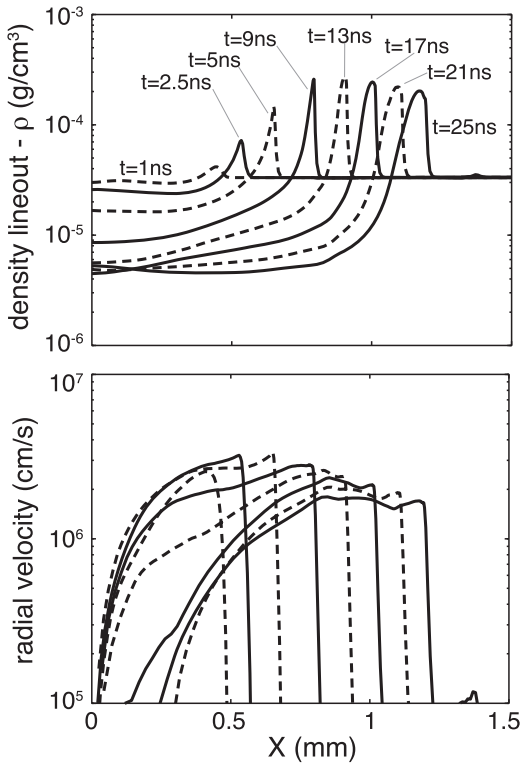

Figure 3. Density and radial velocity evolution for a blast wave launched in Argon with an initial deposited energy of 2 J. several snapshot spanning from early times to late times have been chosen to capture the entire blast wave expansion.

$$\dot{B}_z \propto Ak \sin(k\varphi)\frac{T_e}{L_s}, \tag{5}$$

where $\partial_r T_e \sim T_e/L_s$ is the electron temperature divided by the shock characteristic length L_s. For the BW, in fact, the temperature gradient is radial and peaks in the narrow region of the shock front called *thin shell*. The density gradient in the perturbed region is in the azimuthal direction and therefore orthogonal to the temperature gradient. From equation (5) we deduce that magnetic field has a linear response both in amplitude A and in wavenumber k.

Such bi-linear dependence is well verified in simulations as shown in figures 4(a) and (b). Figure 4(a) presents the linear increase of B for small perturbation amplitude with the mode number l (recalling that in cylindrical geometry $k = l/R$) fixed to 8; while figure 4(b) presents the linear response to mode number for fixed perturbation amplitude A (here set to 3%). We plot the maximum intensity of the B field: the magnetic field is generated only when the shock front passes through the density perturbation, and in this region its value is almost constant. Exiting from the perturbation region, with no sustaining mechanism, the magnetic field is no longer induced while the existing one damps down because of adiabatic expansion. Despite simulations have been run with radiative transfer, two temperatures approximation, NLET thermal diffusion model; the fairly limited thermal precursor dimension permits systematic scans with no saturation effects that instead occurs for higher Z-number material. The bi-linear response with saturation effects for large wavenumber in Argon (Ar) is reported in figures 5(a) and (b). In order to produce a BW with comparable velocity and electron temperature at shock front we require the Ar case to have a specific energy (E/ρ) similar to previous case. For the Ar case the deposited energy is increased to 10 J, and the background gas number density is decreased by a factor of ten, namely $\rho_0 = 5 \times 10^{17}$ cm^{-3}.

An estimate for the B field amplitude generated by the BW in the absence of diffusion can be obtained by integrating equation (5) during the time of transit of the shock front over a fluid element, given by L_s/V_s, where V_s is the shock speed. Recalling $k = l/R$, we obtain

$$B_{max} \propto Ak \cdot \frac{T_e}{V_s} = A\frac{l}{R} \cdot \frac{T_e}{V_s}, \tag{6}$$

which shows that the magnetic field proportionally depends on the electronic shock temperature and perturbation mode-number, while it has an inverse relation with the shock velocity and the perturbation radius R.

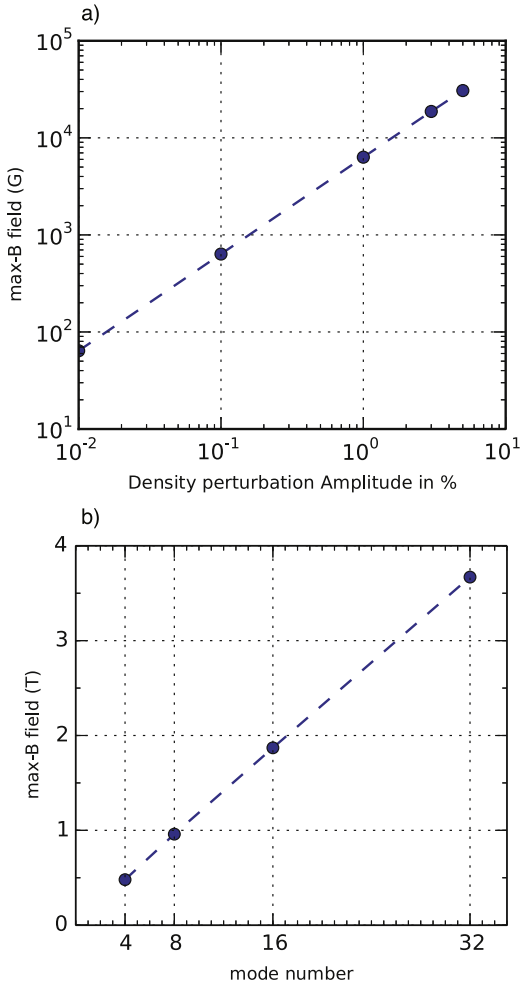

Figure 4. Magnetic field peak value versus density perturbation amplitude (A) express in percent (a) and versus mode perturbation (l) (b). The density background is perturbed with a sinusoidal perturbation of the form $\rho_0(1 + A\cos k\varphi)$ with $\rho_0 = 8.37 \times 10^{-6}$ (Hydrogen, $n_0 = 5 \times 10^{18}$). For plot (a) k is fixed equal to 8 and A is varied; plot (b) assumes $A = 3\%$ and k is chosen equal to $\{4, 8, 16, 32\}$.

We verified equation (6) for increasing BW strength as reported in table 1. Temperature and velocity have been systematically changed by monotonically increasing the deposited energy: from 0.5 to 10 J. The position $R_{\rm pert}$ of the sinusoidal perturbation has been moved progressively outwards in order to allow the BW to stabilize before impinging against the imposed sinusoidal mass perturbation. To verify the scaling relation the case $E = 0.5$ J has been used has a reference point. Last two columns of table 1 show that there is good agreement between the B field peak value and the value predicted by equation (6).

4. Competition between Biermann battery and magnetic field diffusion

To illustrate the competition between the Biermann battery effect and the magnetic field diffusion we proceed by rewriting the induction equation in a dimensionless form [2, 14–16, 36]. We write each dimensional quantity, e.g. the fluid velocity $\mathbf{u}$, in equation (2) as the product of two terms $\mathbf{u} = v_0 \cdot \hat{\mathbf{u}}$, one carrying the physical characteristic dimension v_0, the other the scale $\hat{\mathbf{u}}$. We obtain the dimensionless induction equation

$$\frac{D}{D\hat{t}}\frac{\hat{\mathbf{B}}}{\hat{\rho}} = \frac{\hat{\mathbf{B}}}{\hat{\rho}}\hat{\nabla}\cdot\hat{\mathbf{u}} + \frac{1}{M_{\rm p}}\left(\hat{\nabla}\hat{T}_{\rm e}\times\hat{\nabla}\hat{n}_{\rm e}\right) - \frac{1}{{\rm Re}_M}\left(\hat{\nabla}\times\hat{\eta}\hat{\nabla}\times\hat{\mathbf{B}}\right), \tag{7}$$

where all terms have been reduced to dimensionless form using the characteristic velocity v_0, the characteristic scale length x_0, and the characteristic resistivity η_0.

The relative importance of single terms entering the induction equation can be assessed by studying the *magnetization parameter* $M_{\rm p}$ [35, 36] and the *magnetic Reynolds number* ${\rm Re}_M$ [35–37]. The magnetization parameter is defined by $M_{\rm p} = r_L/x_0$, the ratio of the Larmour radius to the characteristic scale length. Where

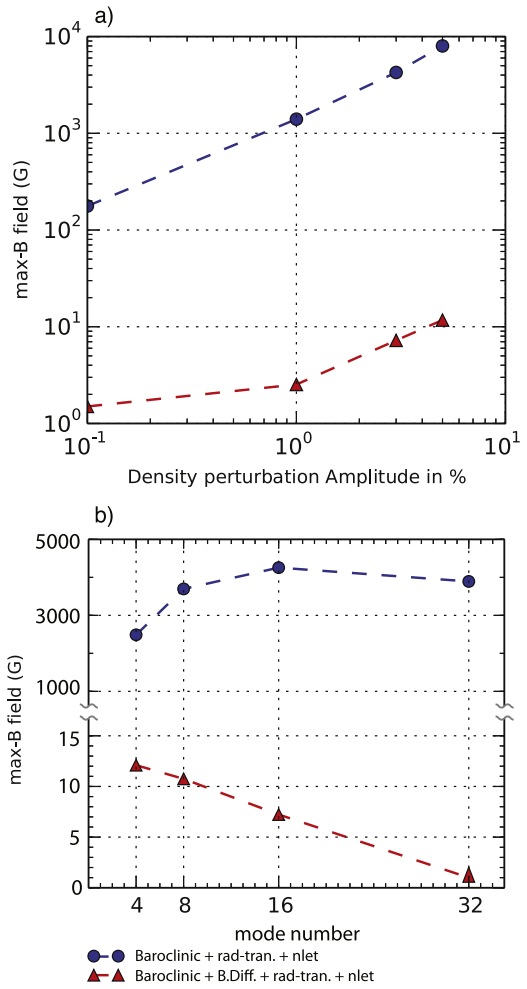

Figure 5. Magnetic field peak value versus: (a) density perturbation amplitude (A) expressed in percent with and without magnetic field diffusivity; (b) versus mode perturbation (l) with and without magnetic field diffusivity. The density background is perturbed with a sinusoidal perturbation of the form $\rho_0(1 + A\cos k\varphi)$ with $\rho_0 = 3.32 \times 10^{-5}$ g cm^{-3} (Argon, $n_0 = 5 \times 10^{17}$ cm^{-3}). For plot (a) k is fixed equal 8 and A is varied; plot (b) assumes $A = 3\%$ and mode-perturbation-l is chosen equal to {4, 8, 16, 32}. The blue dots correspond to magnetic field calculated with the baroclinic source term only; the red triangles correspond to magnetic field calculated with the baroclinic source term plus diffusivity (non local electron transport diffusion for electrons and diffusive approximation radiative transfer are also used).

Table 1. Systematic scan to verify the proportionality $T_e/V_s R_{pert}$ as described in equation (6). The BW has been launched in Argon gas, A is fixed to 1%, l is chosen equal to 16. The deposited energy is increased from 0.5 to 10 J to achieve higher shock velocity.

Energy (J)	V_s (cm s^{-1})	T_e (eV)	R_{pert} (μm)	$\|B\|_\infty$ (T)	Expected B (T)
0.5	3.0×10^6	9	570	0.52	—
1.0	3.5×10^6	10.8	760	0.44	0.40
2.0	3.7×10^6	11.58	1050	0.30	0.29
5.0	4.2×10^6	12.5	1440	0.19	0.2
10.0	5.0×10^6	15.5	1830	0.12	0.15

$M_p \leqslant 1$, the mechanism of B field generation via the baroclinic term becomes important with respect to purely hydrodynamic advection. The magnetic Reynolds number is given by $\mathrm{Re}_M = 4\pi x_0 v_0/(\eta_0 c^2)$, the ratio of magnetic advection to magnetic diffusion. $\mathrm{Re}_M \gg 1$ corresponds to regions of the plasma where diffusion can be neglected and field lines are frozen in flow. On the contrary, $\mathrm{Re}_M \leqslant 1$ indicates that magnetic field diffusion across fluid elements becomes more and more significant.

In the BW expansion, the generation of magnetic field occurs only in the thin shell (magnetization parameter >1, see later on). Therefore we choose to observe the plasma and B field dynamics on the scale of the shock front, and we choose the shock thickness as the characteristic scale length. We also set v_0 to the shock speed

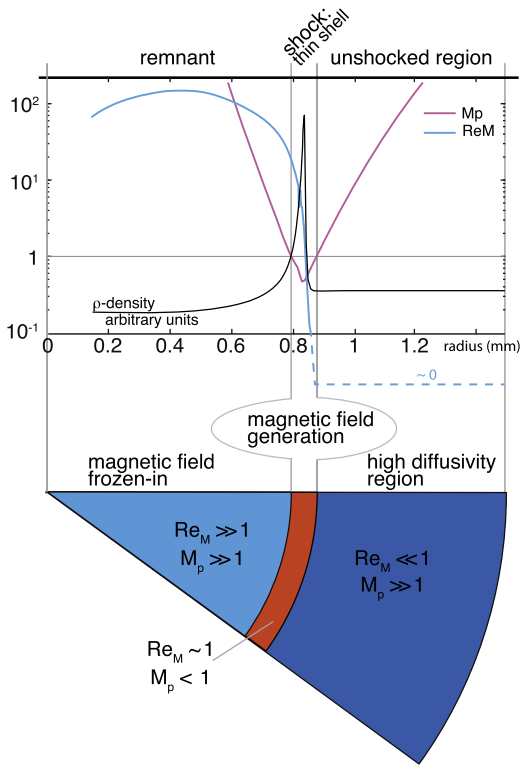

Figure 6. The Magnetization parameter (M_p) and the magnetic-Reynolds (Re_M) number are presented for a blast wave case. The use of dimensionless parameter is a key way to describe the underlying physical mechanism, e.g. magnetic field generation and diffusion. On top, both the M_p and Re_M number are graphed, the density profile in arbitrary units is also reported on the background. The image also shows a simple three zone diagram to highlight from where the magnetic field originates: the shock region (orange stripe); the region of high diffusivity, and the region where the frozen-in-flow approximation holds.

V_s. As a consequence the Re_M and M_p parameters are a function of the local resistivity and of the local Larmor radius respectively, as presented in figure 6. We identify three main regions: the unshocked region ahead of the BW, the shock layer, and the remnant behind the BW. The magnetization parameter is less or equal to one in the thin shell only. There the Biermann battery effect is active. Outside the shock region, instead, M_p is much larger than one and the B field generation is suppressed. Regarding the B diffusion, it can be seen that in front of the shock Re_M is $\ll 1$, so that magnetic diffusion dominates. On the contrary, in the remnant the diffusion is not effective and the B field is frozen in. Just in a very narrow region at the shock front the two dimensionless parameters are both of the order one, and the associated mechanisms are acting with comparable strength.

As a final remark we observe that for a SNR the magnetic Reynolds number is estimated around 3.9×10^{27}. Such a large value arose from the huge scale length involved ($L \sim 3 \times 10^{24}$ cm). Other dimensionless parameters such as the Reynolds number (3×10^{13}) and the Peclet number (7×10^{11}) are also found to have values much greater than unity. The magnetization parameter is instead estimated at around 0.02. The scalability does not rely on having exactly the same values of dimensionless numbers but it suffices that laboratory experiment and astrophysical phenomena have dimensionless numbers in the same range, e.g. larger than one, smaller than one or comparable to unity.

5. Magnetic field diffusivity importance

In the previous section we highlighted the competing effects of magnetic field induction with magnetic field diffusion with the aid of dimensionless parameters, graphically summarized in figure 6. The magnetic field is induced in the thin shock front layer, where diffusivity is also high, so that only a small fraction of the magnetic field is effectively captured. Dimensionless parameters only help us in understanding that the two phenomena are counteracting with similar intensities, but do not offer an effective measurement. In order to calculate the effect that diffusivity has in our specific case, Ar simulations discussed in section 3 have been run with the full equation (2) for **B** evolution. Figure 5 summarizes the comparison. Figure 5 well highlights the importance of diffusivity: when diffusivity is activated the magnetic field reduces from a few tesla to a few gauss. Figure 5(b) denotes an inverse relation with wavenumber: the magnetic field decreases for larger k (this behavior is opposite to the previous case where only magnetic field generation was considered: higher magnetic fields where induced

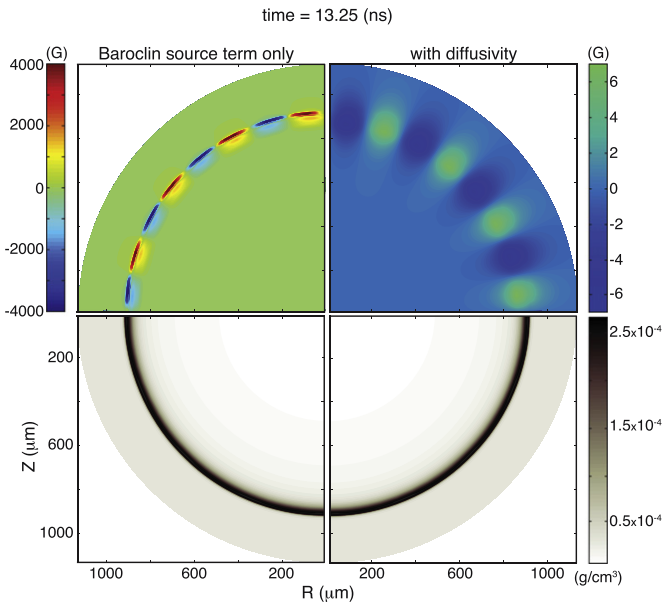

Figure 7. The figure compares the magnetic field induced by an expanding blast wave that impinges into a sinusoidal perturbation in the case where magnetic diffusion is switched off (left panels) and on (right panels). Different colormaps have been used for the two cases, due to the large difference in magnetic field amplitude. Density maps for the two cases are presented on the bottom line.

for larger k). This last relation can be explained from simple considerations. We recall that the density perturbation is of the form $\rho \propto (1 + A)\sin(k\varphi)$ and the induced magnetic field has a form $B_z \propto B_0 \sin(k\varphi)$, where B_0 is the magnetic field amplitude (somehow function of k and A). It follows that

$$\frac{DB_z}{Dt} \propto \left(A\partial_r T_e - \eta B_0 k\right) k \sin(k\varphi). \tag{8}$$

We observe that the diffusive term is proportional to k, so the diffusivity importance increases with k (assuming a slowly varying η).

Figures 7 and 8 offer a visual comparison of the magnetic field intensity and shape (magnetic field topology) for the case with and without diffusivity. Figure 7 corresponds to the case: $l = 16$, $A = 0.03$ $R_{pert} = 800$ μm at 13.25 ns. For figure 7 we have used two distinct colormaps to highlight the different magnitude arising from the two cases, the two colormaps together with the different plot ranges well define the magnetic field spreading-up structure when diffusivity is taken into account. Figure 8 compares the magnetic field induced in the cases where magnetic diffusion is switched off (top panels) and on (bottom panels) for three characteristic times.

6. Random density perturbations

We now consider a different scenario, eventually more realistic, of a BW expanding in a randomly perturbed background gas. We seek to identify a condition that can be reproduced with a moderate laser energy, e.g. the ELFIE laser at LULI Laboratory at the Ecole Polytechnique, and can produce magnetic fields above 100 G. We chose these perturbations to have a gaussian shape, e.g. $A\ \exp\left[-(x - x_0)^2/w^2 - (y - y_0)^2/w^2\right]$, where A (perturbation amplitude), $(x_0,\ y_0)$ (perturbation position) and w (perturbation size) are all randomly guessed. Specifically A can vary in the range $(0,\ 0.8)$, w in the range $(20,\ 50)$ μm, while the perturbation position can be anywhere from $r > 1$ mm (the blast when impinges against the perturbation is well formed in the Sedov–Taylor regime so to avoid any early phase possible kinetic effect that cannot be modelled), figure 9(b). The number of perturbations, for this case, has been fixed to 500. In order to better resolve the imposed perturbations the number of points in the azimuthal direction has been increased to 128. The peak magnetic field for this case is about 140 G, figure 9(a). In order to sustain such a strong magnetic field, density perturbations need to be somehow equally distributed over the entire domain. In the case of density perturbations concentrated in a narrow region the baroclinic source term would generate magnetic fields of the same intensity but for a limited, short, time. Magnetic diffusivity would quickly dominate overall reducing the magnetic fields that would consequently be more difficult to diagnose.

The initial deposited energy is 2 J (e.g. the effective energy for the 2ω laser ELFIE at LULI Laboratory at the Ecole Polytechnique). The blast reaches the perturbation at 8–9 ns. From figure 9(a) we see the formation of a

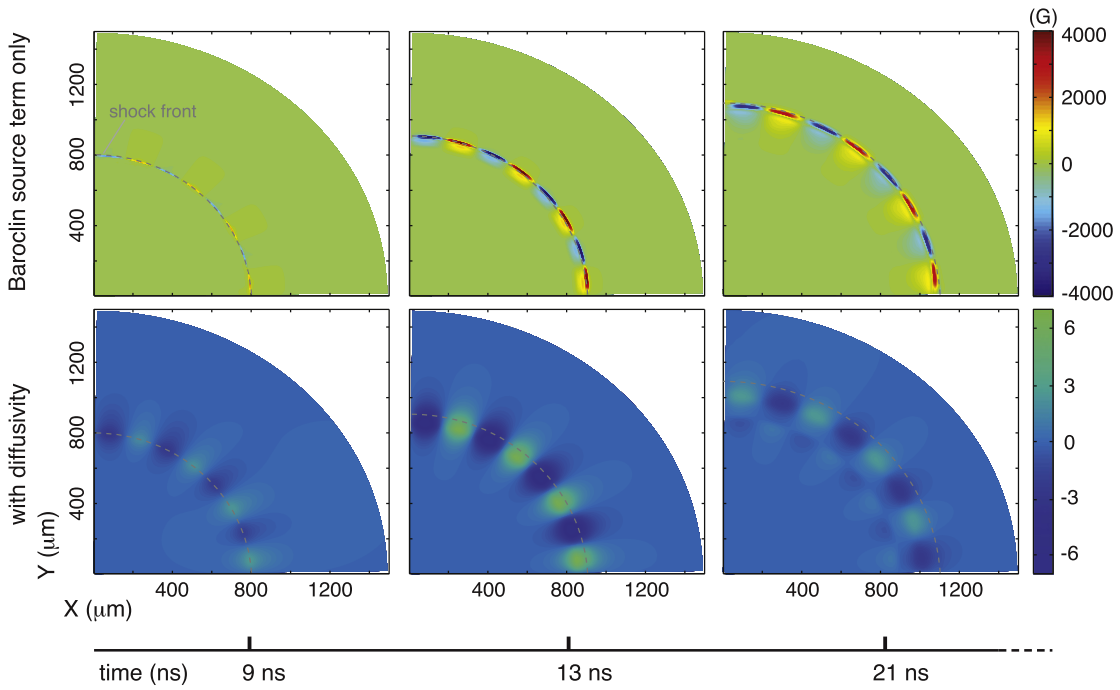

Figure 8. The figures compare the magnetic field induced by an expanding blast wave that impinges into a sinusoidal perturbation for three characteristic times (9, 13, 21 ns) in the cases where magnetic diffusion is switched off (top panels) and on (bottom panels). Different colormaps have been used for the two cases, due to the large difference in magnetic field amplitude.

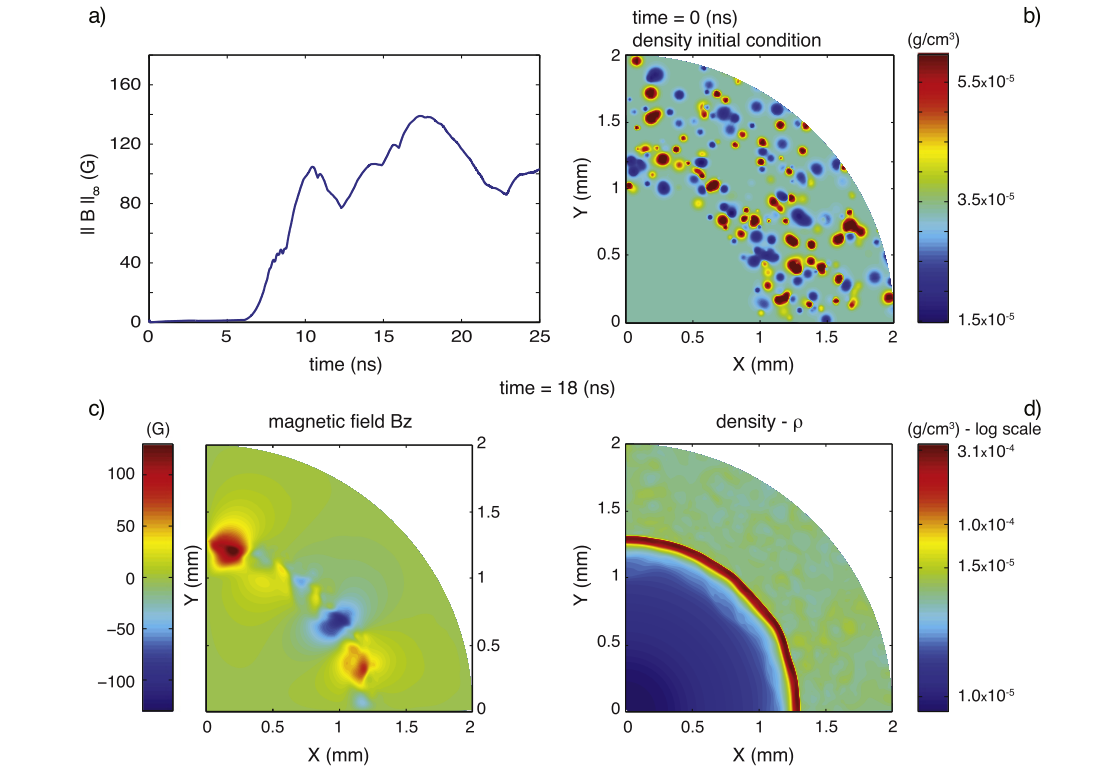

Figure 9. The top-left side of the image, labelled with (a), plots the maximum magnetic field as a function of time. (b) Is the density initial condition: 500 gaussian random perturbations scattered in the region $1 < r < 2$ mm. The bottom part of the graph, label: (c) and (d) are the magnetic field and logarithmic density contour plot respectively, at $t = 18$ ns.

magnetic field of 110 G around that time. Since the random gaussian perturbations permeate the region $r >$ 1 mm the magnetic field is constantly seeded and its value does not decrease below 80 G. Figures 9(c) and (d) display the magnetic field contour and the density contour, respectively, when the magnetic field reaches its peak

value at $t = 18$ ns. We observe from figure 9(c) that the magnetic field has a complex pattern and it appears to have completely lost any reminiscence of the initial density perturbation structure. In other words, the magnetic field topology does not appear to match the initial perturbation pattern. As final remark, we notice that despite the large number of perturbations the BW has still a cylindrical symmetry, (see figure 9(d)).

7. Conclusions

In this paper we have presented the competing effects of the baroclinic source term versus the magnetic field diffusive term in the case of a BW expanding throughout a perturbed background density. We observe that the magnetic field is only induced in the shock region, region also charachterized by a high diffusivity that causes a consequent and fast magnetic field reduction.

A BW expanding in a non-uniform background gas induces a magnetic field. The mechanism that generates, from the electron pressure gradients, such a field is generally referred to as the Biermann battery effect. The magnetic field diffusion contrasts such a mechanism diffusing the magnetic field away. We have verified for a simplified scenario, i.e. for a low-amplitude sinusoidal perturbation, that the baroclinic source term has a bi-linear response both in amplitude and in mode number. When diffusion is also taken into account, we observe that the magnetic field intensity is greatly reduced.

The use of dimensionless parameters is extremely useful for identifying the regions where magnetic field generation and diffusion take place. The magnetic field is only generated at the shock transit where a gradient of temperature and the imposed gradient of density coexist. Only in the shock region M_p is in fact smaller than unity. The induced magnetic field largely diffuses in front of the shock itself since this is a high diffusivity region. The unshocked region is characterized by high M_p parameter and very low Re_M, indicating that there diffusion is the dominant term in B field evolution. The part of the magnetic field that does not diffuse in front of the BW is captured and frozen by the remnant. The remnant is characterized by very high temperatures and very high Re_M so that the frozen-in-flow approximation can be assumed.

We studied also the case of a BW expanding in a randomly perturbed background gas. For such a scenario we observe that the peak magnetic field is of the order of 100 G, and the sparse nature of the perturbation allows the magnetic field to be constantly seeded during the shock evolution. The magnetic field topology is particularly complex and appears to have lost any reminiscence of the initial density perturbation pattern.

Acknowledgments

AM was partially supported by the Italian project FIRB RBFR12NK5K, AS and SA were partially supported by the Italian projects PRIN 2012AY5LEL and Sapienza 2013-C26A13TKPL.

References

[1] Gregori G *et al* 2012 *Nature* **481** 480
[2] Remington B A, Arnett D, Drake R P and Takabe H 1999 *Science* **248** 1488
[3] Symes D R, Comley A J, Tisch J W G and Smith R A 2002 *Appl. Phys. Lett.* **80** 4112
[4] Symes D R 2010 *High Energy Density Phys.* **6** 274–9
[5] Moore A S, Symes D R and Smith R A 2005 *Phys. Plasmas* **12** 052707
[6] Symes D R, Osterhoff J, Fäaustlin R, Maurer M, Bernstein A C, Moore A S, Gumbrell E T, Edens A D, Smith R A and Ditmire T 2007 *High Energy Density Phys.* **3** 353
[7] Moore A S, Lazarus J, Hohenberger M, Robinson J S, Gumbrell E T, Dunne M and Smith R A 2007 *Astrophys. Space Sci.* **1** 139–45
[8] Smith R A, Lazarus J, Hohenberger M, Moore A S, Robinson J S, Gumbrell E T and Dunne M 2007 *Astrophys. Space Sci.* **1** 131–7
[9] Smith R A, Lazarus J, Hohenberger M, Marocchino A, Robinson J S, Chittenden J P, Moore A S, Gumbrell E T and Dunne M 2007 *Plasma Phys. Control. Fusion* **49** 117–24
[10] Remington B A *et al* 1997 *Phys. Plasmas* **4** 1994
[11] Drake R P, Carroll J J, Estabrook K, Glendinning S G, Remington B A, Wallace R and McCray R 1998 *Astrophys. J.* **2** 157–61
[12] Klein R I, Budil K S, Perry T S and Bach D R 2003 *Astrophys. J.* **583** 245–59
[13] Kane J, Arnett D, Remington B A, Glendinning S G, Bazan G, Drake R P, Fryxell B A, Teyssier R and Moore K 1999 *Phys. Plasmas* **6** 2065–71
[14] Ryutov D D, Drake R P, Kane J, Liang E, Remington B A and Wood-Vasey W M 1999 *Astrophys. J.* **518** 821
[15] Ryutov D D, Drake R P and Remington B A 2000 *Astrophys. J. Suppl. Ser.* **127** 465
[16] Ryutov D D, Remington B A, Robey H F and Drake R P 2001 *Phys. Plasmas* **8** 1804–16
[17] Ryutov D D, Drake R P, Kane J, Liang E, Remington B A and Wood-Vasey M 1999 *Astrophys. J.* **518** 821
[18] Robey H F *et al* 2001 *Phys. Plasmas* **8** 2446
[19] Chevalier R A 1984 *Annu. Rev. Astron. Astrophys.* **15** 175–96
[20] Biermann L 1950 *Z. Naturforsch.* Teil A **5** 65
[21] Srinivasan B, Dimonte G and Tang X Z 2012 *Phys. Rev. Lett.* **108** 165002
[22] Séguin F H *et al* 2012 *Phys. Plasmas* **19** 012701
[23] Manuel M J-E *et al* 2013 *Phys. Plasmas* **20** 6301

[24] Haines M G 1986 *Can. J. Phys.* **64** 912
[25] Atzeni S 1986 *Comput. Phys. Commun.* **43** 107
[26] Atzeni S, Schiavi A, Califano F, Cattani F, Cornolti F, Sarto D D, Liseykina T V, Macchi A and Pegoraro F 2005 *Comput. Phys. Commun.* **169** 153
[27] Kuranz C C, Drake R P, Grosskopf M J, Fryxell B, Budde A, Hansen J F, Miles A R, Plewa T, Hearn N and Knauer J 2010 *Phys. Plasmas* **17** 2709
[28] Marocchino A, Atzeni S and Schiavi A 2010 *Phys. Plasmas* **17** 112703
[29] Marocchino A, Atzeni S and Schiavi A 2013 *Phys. Plasmas* **20** 022702
[30] Marocchino A, Atzeni S and Schiavi A 2014 *Phys. Plasmas* **21** 012701
[31] Schurtz G P, Nicolaï P D and Busquet M 2000 *Phys. Plasmas* **7** 4238
[32] Keilty K, Liang E, Remington B, London R, Estabrook K and Kane J 2000 *Astrophys. J. Suppl. Ser.* **127** 375–7
[33] Eidmann K 1994 *Laser Part. Beams* **12** 223
[34] Atzeni S, Caruso A and Pais V A 1986 *Laser Part. Beams* **4** 393
[35] Goldston R J and Rutherford P H 1995 *Introduction to Plasma Physics* (Bristol: Institute of Physics Publishing)
[36] Drake R P 2006 *High-Energy-Density Physics* (Berlin: Springer)
[37] Elsasser W M 1954 *Phys. Rev.* **95** 1